IOP Publishing Journal of Physics D: Applied Physics

J. Phys. D: Appl. Phys. **49** (2016) 075003 (6pp) doi:10.1088/0022-3727/49/7/075003

Micromagnetism of MnBi:FeCo thin films

T H Rana[1,2], P Manchanda[2], B Balamurugan[2], A Kashyap[3], T R Gao[4], I Takeuchi[4], J Cun[5], S Biswas[1], R F Sabirianov[6], D J Sellmyer[2] and R Skomski[2]

[1] Department of Physics, The LNM Institute of Information Technology, Jaipur, Rajasthan, India
[2] Department of Physics and Astronomy and Nebraska Center for Materials and Nanoscience, University of Nebraska, Lincoln, NE 68588, USA
[3] School of Basic Science, Indian Institute of Technology, Mandi, Himachal Pradesh, India
[4] Department of Materials Science and Engineering, University of Maryland, College Park, MD 20742, USA
[5] Energy and Environment Directorate, Pacific Northwest National Laboratory, Richland, WA 99354, USA
[6] Department of Physics, University of Nebraska, Omaha, NE 68182, USA

E-mail: arti@iitmandi.ac.in

Received 2 October 2015, revised 4 January 2016
Accepted for publication 7 January 2016
Published 28 January 2016

Abstract

MnBi:FeCo hard-soft bilayers are investigated using micromagnetic simulations with open boundary conditions and two-dimensional (2D) periodic boundary conditions (PBC). Open and PBC yield similar coercivities of about 1.01 T, in agreement with experiment, but the hysteresis-loop shape is very different in the two theoretical approaches. The difference is ascribed to edge effects, which occur in open boundary conditions but not in PBC and experiment. Near the nucleation field, a curling or vortex mode develops in dots with circular cross sections. The curling mode, which is caused by magnetostatic self-interaction, does not negatively affect the high coercivity of 1.01 T. The magnetostatic self-interaction contributes to the favorable second-quadrant behavior of the MnBi:FeCo thin films.

Keywords: exchanged coupled hard-soft bilayer, micromagnetic, periodic boundary condition, coercivity, hysteresis loop

(Some figures may appear in colour only in the online journal)

1. Introduction

Rare-earth free alternatives to Nd and Sm based permanent magnets have emerged as an urgent technological challenge due to the global economic impact of high and strongly fluctuating rare-earth prices [1–3]. Among possible candidates [4–9], MnBi is one of the few compounds with appreciable intrinsic magnetocrystalline anisotropy, but its low magnetization limits the maximum energy product [12–14]. However, nominal room-temperature energy products of about 200 kJ m^{-3} can be obtained [15] through ferromagnetic exchange coupling between MnBi and Co layers in a unique perpendicular-coupling configuration. This paper focuses on the micromagnetic mechanism of the enhancement, which is similar to that proposed earlier [10, 11] but has the added benefit of an improved hysteresis loop in the second quadrant [15].

While we are approaching the point where it is possible to micromagnetically simulate realistic microstructures [16], there remain challenges. The treatment of extended magnetic systems has, for example with codes such as *Object Oriented Micromagnetic Framework* (OOMMF), been a challenge to micromagnetic simulations. This is because computational cell sizes cannot be arbitrarily large and are normally limited to a very few nanometers or less. At the same time, many nanostructures of scientific and/or technological interest have submicrometer feature sizes. Figure 1 shows one

example, namely demagnetizing effects in 2D and 3D magnets. In the three-dimensional (3D) or bulk case, the demagnetizing-factor concept works due to averaging of magnetic surface charges (top row). In the two-dimensional (2D) or thin-film case (bottom row), the surface charges do not average, the demagnetizing-field approximation breaks down nearly completely and explicit calculations are necessary to treat magnetostatic selfinteraction effects.

A very recent development is the use of periodic boundary conditions (PBC) [17–19] especially for 1D [17] and 2D [19] systems, the PBC added as an extension to OOMMF. Figure 2 illustrates the basic idea of a 2D PBC calculation. The structure of the thin-film magnet is assumed to be periodic, leading to cells labeled by some index i. Magnetostatic dipole interactions between different cells (i and j in figure 2) lead to an Ewald-summation without long distance cut-off. Moreover, each cell has same magnetization as the primary cell and the demagnetizing field can be calculated by recombination of demagnetization tensors. By utilizing the PBC approach, sample-edge effects can be overcome, which is the central theme of this article. In contrast, open boundary conditions may give rise to unphysical edge effects. PBC calculations are now in the process of entering main-stream micromagnetism and increasingly used for complicated problems such as spin waves in thin films [20].

Note that the open-boundary OOMMF code includes magnetostatic interactions, as it includes interatomic exchange interactions. The difference and challenge is that magnetostatic interactions are long-range, so that thin films, nanowires, and bulk materials behave differently. Open boundary conditions assume a finite cut-off radius, beyond which magnetostatic interactions are neglected. They are well-adapted to problems involving surfaces but fail to accurately describe structures that extend to infinity. If the whole film could be 'fed' into a fictitious giant supercomputer, then there would be no need for PBC, but the actual size of regions that can be treated numerically (much smaller than 1 μm) is normally much smaller than the lateral extensions typical experimental systems (several millimeters or centimeters).

Our focus is on the PBC modeling of *two-phase* nanostructures containing MnBi and FeCo. These structures are of interest in the context of exchange-coupled hard-soft nanocomposites for rare-earth-free permanent-magnet applications [10–21]. Recently, Ma *et al* reported the magnetic properties of single phase MnBi as well as MnBi/Fe(Co) composite magnets and found an enhancement in saturation magnetization without sacrificing coercivity when Co nanowires are embedded in MnBi [22].

As a model system, we consider MnBi:FeCo bilayers, where the soft phase provides the high magnetization and the hard phase provides the high anisotropy necessary to stabilize the soft phase and where magnetostatic interactions yield a favorable behavior in the second quadrant of the hysteresis loop [23]. Intrinsically, MnBi shows a high coercive field of 2 T at 450 K, and the magnetic anisotropy increases from 1.2 MJ m^{-3} to 2.4 MJ m^{-3} as the temperature rises from 300 K to 450 K [24]. Moreover, it has a high Curie temperature of about 775 K and a high magnetic moment of about 4 μ_B per Mn atom [25, 26], $Fe_{65}Co_{35}$ alloy has highest room temperature saturation magnetization of 2.45 T [27]. Figure 3 compares the corresponding PBC thin-film geometry with a typical open-boundary structure, namely a nanodot of circular shape. In both cases, the c-axis of MnBi is perpendicular to the film plane, parallel to the external magnetic field **H**.

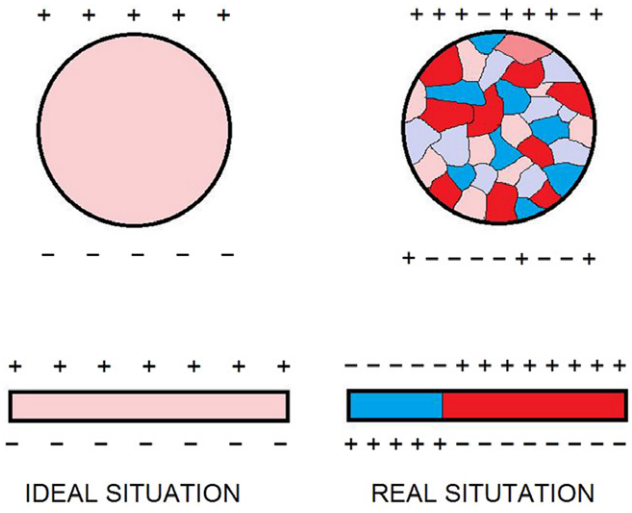

Figure 1. Treatment of demagnetizing-field effects, comparing the demagnetizing-field approximation (left column) with micromagnetic simulations (right column). The top and bottom row refer to 3D (bulk) and 2D (thin-film) magnets. The coloring refers to the magnetization direction: dark red and dark blue mean saturated up and down magnetizations M_z, whereas bright red and bright blue mean small up and down magnetizations, $M_z \approx 0$. (The z-direction is perpendicular to the film plane.)

The present MnBi–FeCo calculation is the first investigation that treats both the magnetization dependence in the z direction perpendicular to the layers and the repetition of structural features in the x–y-plane. Our approach differs from previous calculations of 3D structures, which use open rather than PBC. A good example of the use of open boundary conditions is the description of thin film dots in a recent paper by Oezelt *et al* [28] who consider a single dot, figure 1 in [28].

2. Numerical method and model parameters

An OOMMF simulation [33] solves the LLG (Landau–Lifshitz–Gilbert) equation

$$\frac{\mathrm{d}M}{\mathrm{d}t} = -|\gamma| M \times H_{\mathrm{eff}} - \frac{\alpha|\gamma|}{M_{\mathrm{s}}} M \times (M \times H_{\mathrm{eff}}) \qquad (1)$$

where $\mathbf{M}(\mathbf{r})$ is the local magnetization, $\mathbf{H}_{\mathrm{eff}}$ is the effective magnetic field, γ is the Landau–Lifshitz gyromagnetic ratio, and α is a dimensionless damping constant. We have chosen a value of $\alpha = 0.5$, which leads to fast convergence without any loss in accuracy. In our model, the thicknesses of the hard MnBi and soft FeCo layers are 30 nm and 4 nm, respectively. The lateral size of the dot in figure 3(b) is $100 \times 100\,\mathrm{nm}^2$,

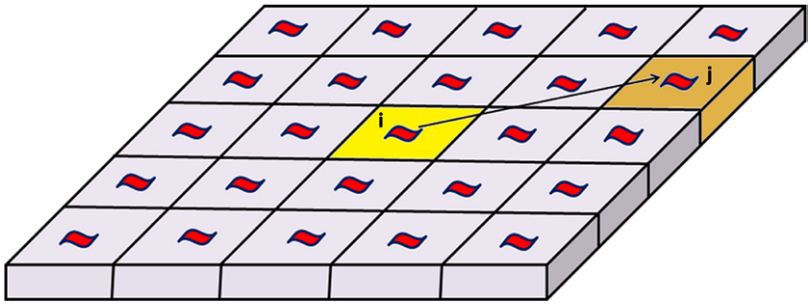

Figure 2. Basic idea of 2D micromagnetic calculation using PBC.

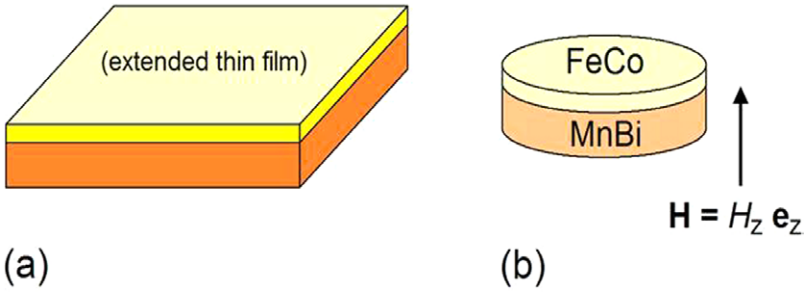

Figure 3. Schematic bilayer exchange-spring model of MnBi:FeCo: (a) thin film with PBC and (b) circular nanodot as an example for open boundary conditions. The thicknesses of the MnBi and FeCo layers are 30 nm and 4 nm, respectively.

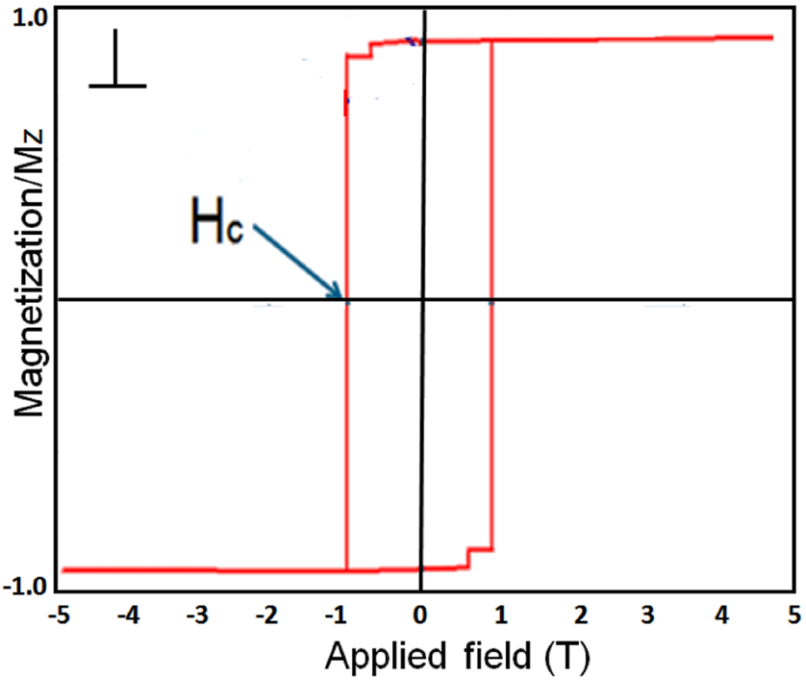

Figure 4. Hysteresis loop for the finite-size nanodot of figure 3(b). The open boundary conditions yield an edge effect, seen as a shoulder in a field of −0.55 T, which is physical for finite dots but unphysical for infinite thin films.

and the length, width and height of each computational cell is $2 \times 2 \times 1\,\text{nm}^3$. The diameter of the disk is 50 nm. An external magnetic field ranging from −5 T to 5 T is applied along the c-axis, as shown in figure 3.

In the simulations, we have used the following values for saturation magnetization M_s, exchange stiffness A, and uniaxial anisotropy constant K_1: $M_s = 0.58$ MA m^{-1} (0.73 T), $A = 8$ pJ m^{-1}, $K_1 = 0.9$ MJ m^{-3} (hard MnBi phase) [29] and

$M_s = 1.91$ MA m^{-1} (2.4 T), $A = 10$ pJ m^{-1}, $K_1 = 0$ (soft FeCo phase) [27]. The interface exchange stiffness was taken as 9 pJ m^{-1}. The parameters taken in the simulations are the same for open and PBC.

3. Results and discussion

3.1. Open boundary condition: hysteresis loop and nucleation modes

We implemented the open-boundary-condition approach for restrictive geometry including magnetostatic interactions between pairs of cells, as in figure 2. Figure 4 shows a typical hysteresis loop for the circular dot of figure 3(b). The small shoulder at −0.55 T is an edge effect caused by magnetization curling. Simple rectangular single-step hysteresis behavior may be due to the nucleation, which start from sample edges. The coercivity obtained by this simulation is 1.01 T, close to the experimental value of 1.3 T [15]. Figure 5 traces the spin structure near the soft surface as a function of the external magnetic field. Figure 5(a) shows the curling mode near the soft-phase nucleation in the second quadrant. With increasingly negative field, the amplitude of the curling mode becomes larger and the magnetization is basically in the x–y-plane. Figures 5(b)–(c) show the magnetizations in the second quadrant near coercivity (b) and at coercivity (c). The formation of the vortex-like curling mode is caused by the micromagnetic competition between exchange energy and magnetostatic energies. At the coercive field, $H_c = -1.01$ T, the magnetostatic interaction dominates and yields curling-like nucleation modes. Such curling or 'vortex' modes are well-known in single-phase magnets [30, 31] but somewhat counterintuitive and virtually unconsidered [32] in two-phase magnets.

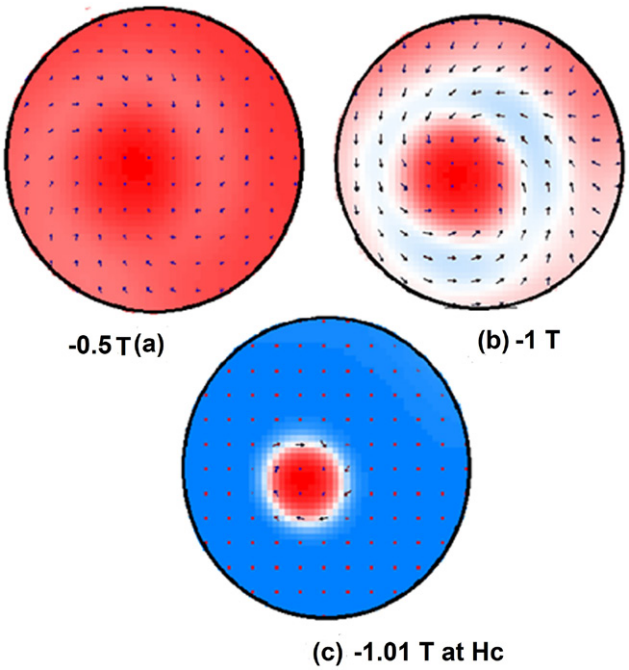

Figure 5. Magnetization curling in circular MnBi:FeCo nanodots during different stages of magnetization reversal: (a) near the nucleation field (and close to remanence, $H = -0.500$ T), (b) in a negative field near coercivity, where much of the soft magnetization is in the film plane ($H = -1.00$ T), and (c) magnetization reversal at coercivity ($H = -1.01$ T). The colors illustrate the magnetization directions (red: magnetization up, blue: magnetization down).

3.2. 2D PBC approach: hysteresis loop and spin structures

Our approach of using 2D PBC is a promising method to study the magnetization reversal in periodic structures. The supercell size is considered 100 × 100 nm^2 for the calculation. Figure 6 shows the hysteresis loop for the film of figure 3(a), calculated with PBC. The coercivity is very similar that derived from figure 4, but the loop shape is different and closer to experiment [15]. A particular feature is the high coercivity (about 1 T), in spite of the very low nucleation field (about −1.5 T). This feature is important, because the energy product is determined by the hysteresis loop in the second quadrant ($H < 0$ and $M > 0$).

The behavior in the second quadrant of figure 6 is a consequence of the layered microstructure. Figure 7 shows the vertical spin configurations of the soft and hard phases during magnetic reversal. The arrows indicate the spin directions but not the magnitudes of the local magnetization. In case of positive magnetic saturation, the spins are well-aligned up to 0.5 T. Figures 7(a)–(c) indicate that the spins start revolving from the top of the soft phase by nucleation. The hard MnBi phase remains largely unaffected at this stage of magnetization reversal. As the magnetic field approaches the coercive field of −1.01 T, figure 7(d), the reversal mode penetrates into the top of the MnBi layer, leading to the flipping of the magnetization of MnBi. Beyond coercivity, at −1.5 T, all the spins in both layers are saturated in the opposite direction, as shown in figure 7(e). The 2D PBC makes the reversal more coherent, but only laterally. Figure 7 explains the high magnetization in the second quadrant, in spite of the low nucleation field. As in all exchange-coupled hard-soft magnets, the hard phase prevents the soft phase from easy switching. An added benefit is the layered structure: the magnetization of the soft phase relatively easily switches into the film plane, due to the strong demagnetizing field $-M_{FeCo}$, but the same demagnetizing field inhibits the further switching the soft region in the second quadrant, between figures 7(c) and (d). The same mechanism is operative in multilayers, because infinite thin-film layers do not interact magnetostatically.

A direct experimental observation of the curling mode is challenging, but preliminary neutron diffraction data [15] may indicate some curling character during magnetization reversal. In fact, such a curling is very likely on physical grounds, because real films are never ideal but exhibit interface roughness and layer-thickness fluctuations. Near coercivity, where the magnetization lies in the film plane, this feature creates magnetic poles and develops a tendency towards curling-like flux closure. For the accurate calculation of the corresponding hysteresis loops, PBC will be indispensable.

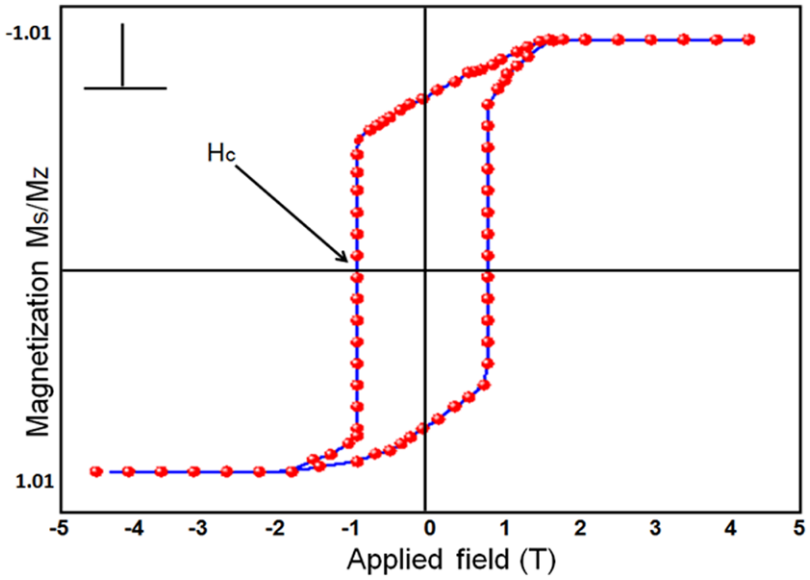

Figure 6. Hysteresis loop obtained with periodic boundary condition.

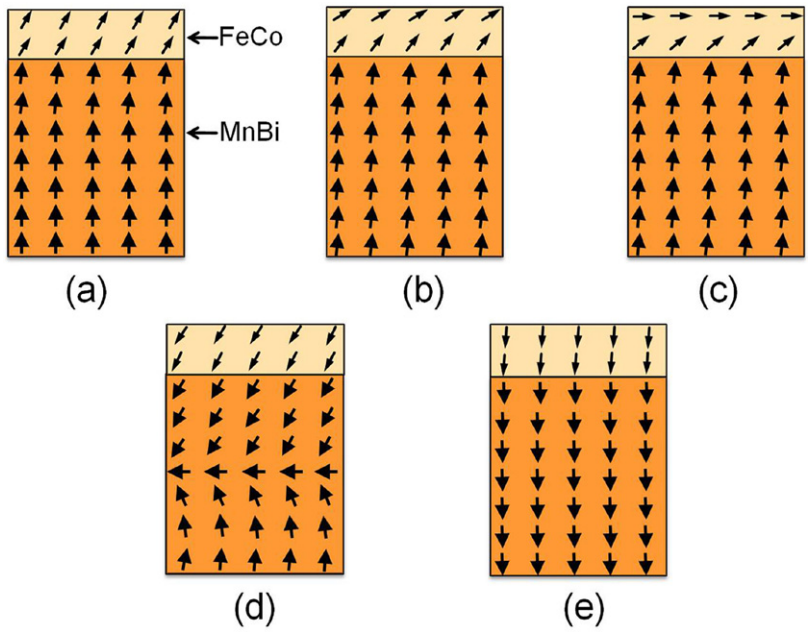

Figure 7. Evolution of vertical spin structure of MnBi:FeCo in different fields during magnetic reversal process: (a) 0.5 T, (b) 0 T, (c) −0.5 T, (d) −1.01 T, and (e) −1.5 T. Only a part of the dot is shown.

4. Conclusions

In summary, we have used micromagnetic simulations with open boundary conditions and PBC to investigate magnetization in MnBi:FeCo thin films. The PBC approach opens the path towards the determination of hysteresis loops without unphysical edge effects. As an example, we have considered magnetization curling, which is realized very differently in periodic and open boundary conditions. In finite dots of circular cross section, the curling occurs automatically, but in extended thin films, it requires structural inhomogeneities. This is of far-reaching importance for the micromagnetic understanding of thin films, as exemplified by MnBi:FeCo hysteresis loops.

Acknowledgment

Thanks are due to W Wang for helpful discussions. This research is supported by PNNL ARPA-E and partially by DREaM (PM) and DOE-BES (FG02-04ER46152, analytical micromagnetism, RS & DJS).

References

[1] Coey J M D 2011 *IEEE Trans. Magn.* **49** 4671–81
Coey J M D 2012 *Scr. Mater.* **67** 524–9
[2] Gutfleisch O, Willard M A, Brück E, Chen C H, Sankar S G and Liu J P 2011 *Adv. Mater.* **23** 821–42
[3] McCallum R W, Lewis L H, Skomski R, Kramer M J and Anderson I E 2014 *Ann. Rev. Mater. Res.* **44** 451–77
[4] Zhou L *et al* 2014 *Acta Mater.* **74** 224–33
[5] Skomski R, Manchanda P, Kumar P, Balamurugan B, Kashyap A and Sellmyer D J 2013 *IEEE Trans. Magn.* **49** 3215–20
[6] Manchanda P *et al* 2013 *IEEE Trans. Magn.* **49** 5194–8
[7] Lewis L H *et al* 2014 *J. Phys.: Condens. Matter* **26** 064213
[8] Lewis L H, Pinkerton F E, Bordeaux N, Mubarok A, Poirier E, Goldstein J I, Skomski R and Barmak K 2014 *IEEE Magn. Lett.* **5** 5500104
[9] Skomski R and Coey J M D 2015 *Scr. Mater.* at press
[10] Kneller E F and Hawig R 1991 *IEEE Trans. Magn.* **27** 3588–600
[11] Skomski R and Coey J M D 1993 *Phys. Rev.* B **48** 15812–6
[12] Rama Rao N V, Gabay A M and Hadjipanayis G C 2013 *J. Phys.* D **46** 062001
[13] Cui J, Choi J P, Li G, Polikarpov E, Darsell J, Overman N, Olszta M, Schreiber D, Bowden M and Droubay T 2014 *J. Phys: Condens Matter* **26** 064212
[14] Skomski R 2003 *J. Phys.: Condens Matter* **15** R841–96
[15] Gao T R *et al* 2015 *Nat. Commun.* submitted
[16] Sepheri-Amin H, Ohkubo T, Gruber M, Shrefl T and Hono K 2014 *Scr. Mater.* **89** 29–32
[17] Lebecki K M, Donahue M J and Gutowski M W 2008 *J. Phys. D: Appl. Phys.* **41** 175005
[18] Fangohr H, Bordignon G, Franchin M, Knittel A, de Groot P A J and Fischbacher T 2009 *J. Appl. Phys.* **105** 07D529
[19] Wang W, Mu C, Zhang B, Liu Q, Wang J and Xue D 2010 *Comput. Mater. Sci.* **49** 84–7
[20] Dmytriiev O, Kruglyak V V, Franchin M, Fangohr H, Giovannini L and Montoncello F 2013 *Phys. Rev.* B **87** 174422
[21] Liu J P, Fullerton E, Gutfleisch O and Sellmyer D J 2009 *Nanoscale Magnetic Materials and Applications* (Berlin: Springer)
[22] Ma Y L, Liu X B, Gandha K, Vuong N V, Yang Y B, Yang J B, Poudyal N, Cui J and Liu J P 2014 *J. Appl. Phys.* **115** 17A755
[23] Skomski R, Manchanda P, Takeuchi I and Cui J 2014 *J. Miner. Metals Mater. Soc.* **66** 1144–50
[24] Kronmüller H, Yang J B and Goll D 2014 *J. Phys.: Condens. Matter* **26** 064210
[25] Guo X, Chen X, Altounian Z and Ström-Olsen J O 1992 *Phys. Rev.* B **46** 14578–82
[26] Yang J B, Yelon W B, James W J, Cai Q, Roy S and Ali N 2002 *J. Appl. Phys.* **91** 7866–8
[27] Bozorth R M 1951 *Ferromagnetism* (Princeton, NJ: Van Nostrand)
[28] Oezelt H, Kovacs A, Wohlhüter P, Kirk E, Nissen D, Matthes P, Heyderman L J, Albrecht M and Schrefl T 2015 *J. Appl. Phys.* **117** 17E501
[29] Coey J M D 2014 *J. Phys.: Condens. Matter* **26** 064211
[30] Brown W F 1963 *Micromagnetics* (New York: Wiley)
[31] Aharoni A 1996 *Introduction to the Theory of Ferromagnetism* (New York: Oxford University Press)
[32] Skomski R, Liu J P and Sellmyer D J 1999 *Phys. Rev.* B **60** 7359–65
[33] Donahue M J and Porter D G 1999 *OOMMF User's Guide, Version 1.0. NISTIR 6376* (Gaithersburg, MD: National Institute of Standards and Technology)